

Accepted Manuscript

Research paper

Nanocrystalline Metal Organic Framework (MIL-101) Stabilized Copper Nanoparticles: Highly Efficient Nanocatalyst for the Hydrolytic Dehydrogenation of Methylamine Borane

Ismail Burak Baguc, Ilknur Efecan Ertas, Mehmet Yurderi, Ahmet Bulut, Mehmet Zahmakiran, Murat Kaya

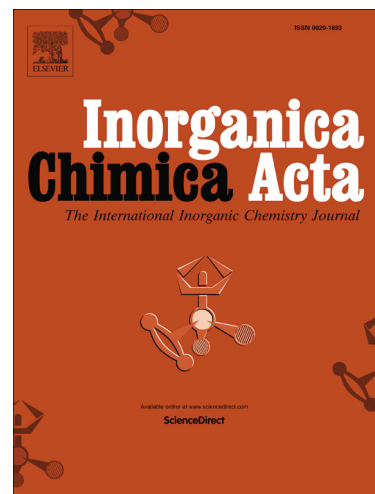
PII: S0020-1693(18)30963-0
DOI: <https://doi.org/10.1016/j.ica.2018.08.056>
Reference: ICA 18456

To appear in: *Inorganica Chimica Acta*

Received Date: 22 June 2018
Revised Date: 30 August 2018
Accepted Date: 30 August 2018

Please cite this article as: I.B. Baguc, I.E. Ertas, M. Yurderi, A. Bulut, M. Zahmakiran, M. Kaya, Nanocrystalline Metal Organic Framework (MIL-101) Stabilized Copper Nanoparticles: Highly Efficient Nanocatalyst for the Hydrolytic Dehydrogenation of Methylamine Borane, *Inorganica Chimica Acta* (2018), doi: <https://doi.org/10.1016/j.ica.2018.08.056>

This is a PDF file of an unedited manuscript that has been accepted for publication. As a service to our customers we are providing this early version of the manuscript. The manuscript will undergo copyediting, typesetting, and review of the resulting proof before it is published in its final form. Please note that during the production process errors may be discovered which could affect the content, and all legal disclaimers that apply to the journal pertain.



Nanocrystalline Metal Organic Framework (MIL-101) Stabilized Copper
Nanoparticles: Highly Efficient Nanocatalyst for the Hydrolytic
Dehydrogenation of Methylamine Borane

Ismail Burak Baguc,^a Ilknur Efecan Ertas,^a Mehmet Yurderi,^a Ahmet Bulut,^a Mehmet Zahmakiran,^{a,*}
Murat Kaya^b

^a Nanomaterials and Catalysis Research Group, Department of Chemistry, Yuzuncu Yil University,
65080, Campus, Van, Turkey

^b Department of Chemical Engineering and Applied Chemistry, Atilim University, 06836, Ankara, Turkey

*Corresponding author: Prof. Mehmet Zahmakiran; zmehmet@yyu.edu.tr; www.nanomatcat.com

Abstract

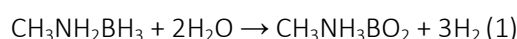
The copper nanoparticles stabilized by nanocrystalline MIL-101 framework (Cu/nano-MIL-101) was reproducibly prepared by following double solvent method combined with liquid phase chemical reduction technique. The characterization of the resulting new material was done by using various analytical techniques including ICP-OES, P-XRD, N₂-adsorption-desorption, XPS, FE-SEM, SEM-EDX, BFTEM and HAADF-STEM; the summation of their results reveals that the formation of well-dispersed and very small sized (0.8 nm) copper nanoparticles within nanocrystalline MIL-101 framework. The catalytic performance of Cu/nano-MIL-101 in terms of activity and stability was tested in the hydrolytic dehydrogenation of methylamine borane (CH₃NH₂BH₃), which has been considered as one of the attractive materials for the efficient chemical hydrogen storage. Cu/nano-MIL-101 catalyzes the hydrolytic dehydrogenation of methylamine borane with high activity (turnover frequency; TOF = 257 mol H₂/mol Cu×h) and conversion (> 99 %) under air at room temperature. Moreover, these nano-MIL-101 framework stabilized copper nanoparticles show great durability against to sintering and leaching, which make Cu/nano-MIL-101 reusable nanocatalyst in the hydrolytic dehydrogenation of methylamine-borane. Cu/nano-MIL-101 nanocatalyst retains 83 % of its inherent activity at complete conversion even at 10th recycle in the hydrolytic dehydrogenation of methylamine borane.

Keywords: Methylamine borane; Metal organic framework; Copper; Dehydrogenation; Hydrogen.

1. Introduction

In the view of a desirable and drastic reduction of world-wide greenhouse gas emissions, the utilization of sustainable energy sources are a mandatory option in the world energy consumption [1, 2]. In the context of new advanced energy conversion technologies, since the 1990's a strong interest from the international scientific and industrial community has been addressed towards the possible development of 'Hydrogen Economy' based on the hypothesis that hydrogen (H₂) could play a crucial role as a secondary fuel and energy carrier in the new energy system [3, 4]. H₂ has a high volumetric hydrogen density of 53 g.L⁻¹, that satisfies the 2017 target of 40 g.L⁻¹ for on-board hydrogen storage target recently announced by the U.S. Department of Energy (DOE) [5] and can efficiently be converted into energy in an internal combustion engine or fuel cells with the production of water as the only by-product [3, 4]. However, dramatic improvements in the existing technologies especially for the controlled storage and release of H₂ are still needed, if hydrogen is to become a major energy vector in the near future [6, 7].

At this concern, a numerous studies have been performed for the development of materials with high volumetric and gravimetric hydrogen storage capacity, as the low density of hydrogen makes it difficult to store in compressed or liquefied form [8]. In line with this, various porous materials [9-12], boron based chemical hydrides [13-15] and boron-nitrogen compounds [16-20] have been tested for the chemical hydrogen storage. Amongst these materials ammonia-borane (NH₃BH₃) has recently received the greatest interest because of its 19.6 wt % hydrogen content, and its being highly stable and environmentally benign [17]. However, the methyl-substituted ammonia-borane, methylamine borane (CH₃NH₂BH₃, MeAB) with the 11.1 wt % hydrogen content, has not been widely studied [22-31]. To date, thermal decomposition in the solid state [21, 22] or metal-catalyzed dehydrocoupling [23, 31] in the organic medium have been demonstrated to provoke the hydrogen release from MeAB. Although, difficulties in the regeneration of hydrolysis products due to the strong B-O bonds, there is much interest in the transition-metal-catalyzed hydrolytic dehydrogenation of MeAB due to favorable fast hydrogen generation under mild reaction conditions [24-30]. The results of the studies concerned with the metal-catalyzed hydrolysis of MeAB [24-30] have already showed that ~3 equiv. of H₂ per mole of MeAB can be generated from the aqueous solution of MeAB (Eq. 1) in the presence of a suitable catalyst under mild conditions (at RT under air).



The hydrolytic dehydrogenation of MeAB has significant advantages: (i) MeAB is highly stable in aqueous solution against to self-hydrolysis, (ii) the hydrolytic dehydrogenation of MeAB occurs at appreciable rates only in the presence of suitable catalysts, (iii) the hydrolytic dehydrogenation of MeAB generates 3 moles of H₂ per mole of MeAB (Eq. 1). Up to date, the catalysts tested in the

hydrolytic dehydrogenation of MeAB are graphene supported core@shell type Ag@M (M= Co, Ni, Fe) nanoparticles (NPs) [25], Cu@Co NPs [26], Ag@CoNi NPs [27], Ru@Co NPs [28], Ru@Ni NPs [29] and MCM-41 encapsulated Ru NPs [30]. Among these catalytic architectures Ru based systems [28-30] provide high activities in the hydrolytic dehydrogenation of MeAB. However, the concerns over the practical usage of these high cost metals have motivated the research for the development of low cost and active catalyst systems for this important reaction.

As seen from the previous attempts, the active catalytic systems involves transition metal NPs, which have higher surface-to-volume ratio comparing to bulk counterparts, thus, larger fraction of catalytically active atoms exist on their surface [32]. For all that metal NPs are considered as thermodynamically unstable against to agglomeration into bulk form due to their large surface areas and high surface energies. At this concern, the suitable protecting ligands or polymers are widely used in their synthesis to avoid their aggregation [33]. However, the agglomeration of metal NPs eventually to the bulk form even in the presence of best stabilizing agents [34] is still the most vital concern that should be overcome in their catalytic applications. Additionally, it is another critical matter to obtain pure active metal surfaces by staying away from surface contamination resulting from surface protecting groups, which often lead to a decrease in the catalytic activity resulting from the blocking of active sites. In this context, the utilization of porous solid matrices as host material for the immobilization of guest metal NPs allows the generation of specific surfactant-free active sites with the advantages of preventing particle aggregation [32-34].

In this context, porous solid support materials like zeolites [35, 36], carbon based materials [37, 38], and minerals [39, 40] have been widely used to synthesis of stable metal NPs within their porous matrices [41]. Besides these porous materials, more recent studies [42, 43] have also indicated that metal-organic frameworks (MOFs), which are highly crystalline hybrid materials that combine metal ions with rigid organic ligands [44], can also be considered as suitable host materials to stabilize guest metal NPs. Indeed, MOFs can be used as more suitable support material for metal NPs with respect to other porous solids as they allow more flexible and systematic modification of the pore structure by the proper selection of the structural subunits and their connected way ligands [42-44]. Moreover, the stabilization of metal NPs within the structure of MOFs produces solid catalytic materials, which can help us in the kinetic control of the catalytic reactions. In this context, the selection of MOFs type properly depending on the reaction conditions is the most critical step for the employment of MOFs as supports for metal NPs immobilization as only a few MOFs with suitable pore structures are presently known for their thermal/chemical stability. In this line, the results of recent studies have shown that chromium(III) terephthalate ($[\text{Cr}_3\text{F}(\text{H}_2\text{O})_2\text{O}\{\text{O}_2\text{CC}_6\text{H}_4(\text{CO}_2)\}_3 \cdot n\text{H}_2\text{O}]$) framework; MIL-101; MIL: Materials Institute Lavoisier), which was first reported in *Science* paper by Ferey and co-

workers in 2005 [45], can be used as a suitable host material for the stabilization of guest metal NPs as it is stable in water even under very acidic conditions and can show thermal stability up to 300 °C under air [18]. MIL-101 has a large surface area ($\sim 4100 \text{ m}^2 \cdot \text{g}^{-1}$) and contains two different types of cages with diameters of 29 and 34 Å, which have pore apertures of 12 and 16 Å, respectively. These unique properties of MIL-101 have encouraged us to focus on the use of the MIL-101 matrix in catalysis [46-49] for the stabilization of transition metal NPs [50-52]. Our previous studies have already shown that MIL-101 is suitable support material for the fabrication of catalytically active Ru [53] and Rh [54] NPs for the selective hydrogenation of phenol to cyclohexanone. In this study we decided to use nanocrystalline MIL-101 as host material to guest copper NPs. The reduction of the MIL-101 matrix particle size from the microcrystalline to the nanocrystalline regime (from $>1 \mu\text{m}$ to $<100 \text{ nm}$) was performed in anticipation of improved activity due to lower mass transfer limitations for liquid-phase dehydrogenation of MeAB at low temperature [40, 55].

Herein, we report the synthesis, characterization and catalytic application of copper NPs stabilized by nanocrystalline MIL-101 framework, hereafter referred to as Cu/nano-MIL-101, in the hydrolytic dehydrogenation of MeAB. Cu/nano-MIL-101 nanocatalyst was reproducibly prepared by the double solvent method [56, 57] combined with the liquid phase chemical reduction technique [41] all at room temperature. The characterization of Cu/nano-MIL-101 was done by using various analytical techniques including inductively coupled plasma-mass spectroscopy (ICP-MS), powder X-ray diffraction (P-XRD), Fourier transform infrared spectroscopy (FTIR), X-ray photoelectron spectroscopy (XPS), diffuse reflectance UV-vis spectroscopy (DR-UV-vis), field-emission scanning electron microscopy (FE-SEM), scanning electron microscopy-energy dispersive X-ray spectroscopy (SEM-EDX), bright field transmission electron microscopy (BFTEM), high-resolution transmission electron microscopy (HRTEM), scanning transmission electron microscopy-energy dispersive X-ray spectroscopy (STEM-EDX) and high-angle annular dark field-scanning transmission electron microscopy (HAADF-STEM). The summation of the results gained by these aforementioned analyses, points toward the formation of well-dispersed and small-sized copper NPs nucleated within the framework of nano-MIL-101 support material.

The resulting catalytic architecture, Cu/nano-MIL-101, catalyzes hydrolytic dehydrogenation of MeAB under mild conditions (at room temperature and under air). Cu/nano-MIL-101 nanocatalyst affords remarkable turnover frequency (TOF = $257 \text{ mol H}_2/\text{mol Cu}_x\text{h}$ at 25 °C) and conversion ($> 99 \%$) in the hydrolytic dehydrogenation of MeAB. The small size of the resulting copper-copper oxide NPs and their surfactant-free clean surface should account for their high catalytic activity. Moreover, the high stability of these new supported copper-copper oxide NPs against agglomeration and leaching

turns Cu/nano-MIL-101 into an excellent candidate for a long-lived and recyclable heterogeneous catalyst, in the hydrogen production from MeAB for on-board fuel cell applications.

2. Experimental

2.1 Chemicals and materials

Chromium(III) nitrate nonahydrate, terephthalic acid ($C_8H_6O_4$), methanol (CH_3OH), acetone (CH_3COCH_3), sodium borohydride ($NaBH_4$), copper(II) chloride dihydrate ($CuCl_2 \cdot 2H_2O$), methylamine hydrochloride ($CH_3NH_2 \cdot HCl$), tetrahydrofuran (C_4H_8O) and diethyl ether ($(CH_3CH_2)_2O$) were purchased from Sigma-Aldrich. Deionized water was distilled by water purification system (Milli-Q Water Purification System). All chemicals were used as received and without further purification. Micron sized MIL-101 [58], nanocrystalline MIL-101 [59] and MeAB [25-29] were synthesized according to literature procedures. The catalytic materials isolated at the end of the synthesis were stored in a Labsconco nitrogen atmosphere glovebox ($H_2O < 5$ ppm, $O_2 < 1$ ppm). Deionized water was distilled through the water purification system (Milli-Q Water Purification System). All glassware and Teflon-coated magnetic stirring bars were washed with acetone and copiously rinsed with distilled water before drying in an oven at $150^\circ C$.

2.2. Characterization

Copper (Cu) contents of the samples were determined by ICP-MS (Perkin Elmer DRC II model) after each sample was completely dissolved in a mixture of HNO_3/HCl ($v/v = 1/3$). Powder X-ray diffraction (XRD) patterns were recorded with a Rigaku Ultima IV diffractometer using $Cu-K\alpha$ radiation (wavelength 1.54 \AA , 40 kV , 55 mA). FE-SEM analyses was done by using Quanta 400F field emission SEM. BFTEM, HRTEM, STEM, and HAADF-TEM samples were prepared by dropwise addition of the dilute catalyst suspension on a copper-coated carbon TEM grid followed by the evaporation of the solvent. The conventional TEM measurements were carried out on a JEOL JEM-200 CX transmission electron microscope operating at 120 kV . HRTEM, STEM, and HAADF-STEM analysis were performed using a JEOL JEM-2010F transmission electron microscope operating at 200 kV . Oxford EDX system and the Inca software were exploited to acquire and process STEM-EDX data. The XPS measurements were employed via a Physical Electronics 5800 XP spectrometer equipped with a hemispherical analyzer and a monochromatic $Al K\alpha$ X-ray source (1486.6 eV , 15 kV , 350 W , with pass energy of 23.5 eV). NMR spectra were recorded on Bruker Avance DPX 400 MHz spectrometer (400.1 MHz for 1H NMR; 128.2 MHz for ^{11}B NMR). $BF_3 \cdot (C_2H_5)_2O$ was used as the external reference for ^{11}B NMR chemical shifts.

2.3. Cu/MIL-101 and Cu/nano-MIL-101 preparation

Cu/MIL-101 and Cu/nano-Mil-101 catalysts were prepared through double solvent method [49, 50] followed by wet- chemical reduction [41]. Typically, 200 mg support material (MIL-101 or nano-MIL-101) was suspended in 10 mL dry *n*-hexane as hydrophobic solvent and the mixture was sonicated for 15 min. then taken on magnetic stirrer and stirred at 700 rpm at room temperature. After stirring of 1 h, 1.0 mL aqueous $\text{CuCl}_2 \cdot 2\text{H}_2\text{O}$ (17.04 mg, 0.1 mmol Cu) was added dropwise over 10 min. with constant stirring for 2 hours. After centrifugation (6000 rpm, 10 min.), copious washing with water (3×10 mL), the isolated sample in powdered form was dried in a vacuum oven (10^{-1} Torr) at 70 °C for 3 h. Then, the isolated and purified powder sample was added into 2.0 mL aqueous solution of NaBH_4 and this mixture was stirred for half an hour under ambient conditions. Next, the mixture was centrifuged (3000 rpm, 5min.), washed with water (3×10 mL) and dried in a vacuum oven (10^{-1} Torr) at 70 °C for 3 hours. Finally, Cu/MIL-101 and Cu/nano-MIL-101 catalysts in dark-gray powder form was stored in a Labsconco nitrogen atmosphere glovebox ($\text{H}_2\text{O} < 5$ ppm, $\text{O}_2 < 1$ ppm).

2.4. Hydrolytic dehydrogenation of MeAB

The hydrolytic dehydrogenation of aqueous MeAB solution was surveyed by volumetric measurement of the rate of hydrogen evolution. The volume of released gas during the reaction was monitored using a gas burette through water displacement as described elsewhere [14, 20, 35-36]. Beforehand starting, a jacketed one-necked Schlenk tube (20.0 mL), of which the temperature was adjusted by circulating water through the jacket from a constant temperature bath, containing a Teflon-coated stirring bar was placed on a magnetic stirrer. In a typical catalytic activity test, catalyst was weighed and transferred to the Schlenk, and then 8.0 mL H_2O was added into this Schlenk followed by rigorous stirring for 15 mins to achieve a thermal equilibrium. Next, 2.0 mL of aqueous MeAB solution (100 mM in 10.0 mL H_2O) was added into the reaction flask via its septum using a 1.0 mL gastight syringe, and the catalytic reaction was started ($t = 0$ min) by stirring the mixture at 900 rpm.

2.5. Kinetic studies for Cu/nano-MIL-101 catalyzed hydrolytic dehydrogenation of MeAB

In a series of experiments, the hydrolytic dehydrogenation of MeAB ($[\text{MeAB}] = 100$ mM) was carried out 25.0 °C starting with different initial concentrations of Cu (51, 34, 17 and 8.5 μmol) in Cu/nano-MIL-101. Next, to obtain activation energy (E_a) the hydrolytic dehydrogenation of MeAB ($[\text{MeAB}] = 100$ mM) in the presence of Cu/nano-MIL-101 (Cu = 17 μmol) was performed at different temperatures (15, 25, 35 and 45 °C).

2.6. Catalytic stability measurements

The catalytic stability of Cu/nano-MIL-101 in the hydrolytic dehydrogenation of MeAB was assessed via catalytic recyclability experiments. The recyclability of Cu/nano-MIL-101 in the hydrolytic dehydrogenation of MeAB was determined by a series of experiments started with a 10.0 mL aqueous

FA solution (0.22 M in 10.0 mL H₂O) at room temperature. Instantaneously after the achievement of > 90 % conversion in the 1st catalytic run, another equivalent amount of fresh MeAB was added to the reaction mixture, leading to further hydrogen evolution.

3. Results and discussion

3.1. Preparation and characterization of Cu/nano-MIL-101

Cu/nano-MIL-101 catalyst was prepared with high reproducibility by following a method, which comprised of a double solvent method [56, 57] combined with a liquid phase chemical reduction technique [41]. The dark gray solid powdered samples of Cu/nano-MIL-101 yielded at the end of the synthesis protocol were characterized by multipronged advanced analytical techniques. Firstly, the crystallinity of the host material at various copper loadings was investigated by P-XRD analyses. **Fig. 1** shows P-XRD patterns of the host material (nano-MIL-101) and Cu/nano-MIL-101 samples at different copper loadings (wt % Cu = 1.09, 2.18 and 4.12 as determined by ICP-OES). P-XRD-patterns of Cu/nano-MIL-101 samples at all Cu loadings are almost identical to that of the host nano-MIL-101 framework, thus indicating that no new phases appear and plus neither the crystallinity nor the lattice of nano-MIL-101 was essentially altered by the formation of Cu/nano-MIL-101. The absence of any Bragg peaks assignable to Cu NPs can be attributed to their low amount of loading onto host material. Additionally, the slight decrease in the intensity of Bragg peaks in Cu/nano-MIL-101 samples by the increase of Cu loading can be explained by the changes in the charge distribution and electrostatic fields as a result of the existence of Cu NPs on the surface and interaction of their electrophilic surface with framework atoms [60].

XPS provides further insights to the oxidation state of copper and surface composition of the resulting Cu/nano-MIL-101. The survey scan XPS spectrum of Cu/nano-MIL-101 sample is depicted in **Fig. 2(a)**, which shows the existence of MIL-101 framework elements (Cr, O and C) and Cu. The existence of Na and B signals indicative of the presence of surface bound contaminated sodium (Na⁺) and metaborate (BO₂⁻) ions most probably came from hydrolysis of NaBH₄, which was used as reducing agent. The high resolution Cu 2p XPS (HR-XPS) spectrum of Cu/nano-MIL-101 sample (2.18 wt % Cu loading) and its deconvolution are given in **Fig. 2(b)**. The deconvolution of high resolution Cu 2p XPS spectrum of Cu/nano-MIL-101 sample gives a distinctive peak at 931 eV that can readily be assigned to metallic Cu(0) [61]. The peaks observed at 933 and 935.5 eV reveals the presence of CuO phase, which may originate from the surface oxidation of Cu(0) NPs during the XPS sampling procedure [62, 63].

Nitrogen adsorption–desorption isotherms of nano-MIL-101 and Cu/nano-MIL-101 are given in **Fig. 3** and they show type I shape isotherm, which is a characteristic of microporous materials [64].

The micropore volume and area were determined for nano-MIL-101 and Cu/nano-MIL-101 by the t -plot method [65]. The appreciable decrease in the micropore volume (from 1.42 to 1.12 cm³/g) and BET-surface area (from 3044 to 2586 m²/g) on passing from nano-MIL-101 to Cu/nano-MIL-101 can be explained by blocking of the windows of cavities by the deposition of Cu(0) NPs exist mainly on the surface of nano-MIL-101; as the electron microscopy analyzes (*vide infra*) show the existence of Cu(0) NPs supported on the surface of nano-MIL-101.

FE-SEM, SEM-EDX, BFTEM and HAADF-STEM analyses were performed to examine the size, morphology and the composition of Cu/nano-MIL-101. FE-SEM images of Cu/nano-MIL-101 sample (2.18 wt % Cu loading) from different regions in different magnifications are given along with SEM-EDX spectrum in **Fig. S1** (in the Supporting Information). These images are indicating that (i) there exist only crystals of nano-MIL-100, (ii) there is no bulk copper metal formed in observable size outside MIL-101 nanocrystals. Although no bulk copper metal is observed outside MIL-101 nanocrystals, SEM-EDX and ICP-OES analyses reveal that the presence of copper in the sample, which implies that the formation of very small sized and unagglomerated Cu NPs. Expectedly, BFTEM images of Cu/nano-MIL-101 sample (2.18 wt % Cu loading) given in **Fig. 4(a)-(d)** displays highly crystalline nano-MIL-101 host material and very small sized Cu(0) NP, the mean particle size of the resulting Cu(0) NP was found to be 0.8 ± 0.3 nm by the particle size analysis of > 50 non-touching Cu(0) NP. The existence of Cu NPs was also confirmed by HAADF-STEM analysis of the same sample, bright spots observed in the HAADF-STEM image (given in the inset of Fig. 4(c)) of the selected region given in Fig. 4(c) shows the presence of very small sized slightly clumped Cu NPs within the framework of nano-MIL-101 host material.

3.2. Catalytic reactivity of nano-MIL-101 and effect of Cu loadings on the catalytic activity of Cu/nano-MIL-101 in the hydrolytic dehydrogenation of MeAB

MIL-101 metal organic framework has Cr(III) Lewis acidic sites and it has recently been reported that Lewis acid catalyst can promote the evolution of up to 2.5 equivalents of H₂ from our substrate (MeAB) analogous ammonia-borane (NH₃BH₃) molecule [66]. For this reason, before testing the catalytic activity of Cu/nano-MIL-101, the catalytic reactivity of the host material nano-MIL-101 was examined under the same conditions (*vide infra*). The result of this experiment showed that the host material nano-MIL-101 is catalytically inactive in the hydrolytic dehydrogenation of MeAB.

As the next, the hydrolytic dehydrogenation of MeAB was performed by using Cu/nano-MIL-101 samples with different copper loadings in the range of 1.09–4.12 wt % by keeping the copper concentration identical (in all [Cu] = 3.44 mM) to determine the effect of copper loading on the catalytic activity of Cu/nano-MIL-101. **Fig. 5** shows mole of evolved H₂/mole of MeAB versus time graph for these Cu/nano-MIL-101 samples catalyzed hydrolytic dehydrogenation of MeAB at room

temperature. As seen from this graph, the highest catalytic activity was obtained by Cu/nano-MIL-101 sample with 2.18 wt % copper loading. The variation in catalytic activity reflects the accessibility of Cu(0) NPs in the nano-MIL-101 framework by the substrate so in the Cu/nano-MIL-101 sample with 2.18 wt % copper loading most of the Cu NPs on the surface and readily accessible by MeAB. The small size of Cu/nano-MIL-101 containing 2.18 wt % Cu may be another reason for its high activity with respect to that of containing 4.12 wt % Cu. Expectedly, an informative BFTEM (**Fig. S2** in the Supporting Information) taken from Cu/nano-MIL-101 sample containing 4.12 wt % Cu shows the existence of slightly larger size (> 2.0 nm) Cu NPs on the surface of Cu/nano-MIL-101. For all the tests reported hereafter, the copper loading used was ~ 2.18 wt % unless otherwise stated. The $^{11}\text{B}\{-^1\text{H}\}$ -NMR spectrum (**Fig. S3** in the Supporting Information) taken from the reaction solution at the end of the dehydrogenation of DMAB (when no more hydrogen is evolved) shows that MeNH_2BH_3 ($\delta=-19$ ppm, q) is completely converted to methylammonium borate (MeNH_3BO_2 ($\delta=-13.8$ ppm, s)).

3.3. Effect of the size of host material on the catalytic activity of the guest Cu(0) NP: The comparison of the catalytic activity of Cu/nano-MIL-101 and Cu/MIL-101 in the hydrolytic dehydrogenation of MeAB

A decrease in the particle size of host material from microcrystalline (>1 μm) to nanocrystalline (<100 nm) results in high external surface areas, which increases the possibility of formation of small size surface bound Cu(0) NPs, and thus, reduces the diffusion path length compared to the large size MIL-101 crystals. With this anticipation, we employed nano-MIL-101 as host material for guest Cu(0) NPs. In order to investigate the effect of size of host material on the catalytic activity of MIL-101 stabilized Cu(0) NPs in the hydrolytic dehydrogenation of MeAB, we compared the catalytic activities of Cu/nano-MIL-101 (2.18 wt % Cu loading) and Cu/MIL-101 (2.21 wt % Cu loading), which were prepared by following the same synthesis protocol, by keeping the copper concentration same (in all $[\text{Cu}] = 3.44$ mM) in the hydrolytic dehydrogenation of MeAB.

Fig. 6 shows mole of evolved H_2 /mole of MeAB versus time graph for Cu/nano-MIL-101 (2.18 wt % Cu loading) and Cu/MIL-101 (2.21 wt % Cu loading) catalyzed hydrolytic dehydrogenation of MeAB at room temperature. Expectedly, as seen from this graph Cu/nano-MIL-101 (2.18 wt % Cu loading) catalyst provides better catalytic performance in terms of activity and conversion than Cu/MIL-101 (2.21 wt % Cu loading) in the hydrolytic dehydrogenation of MeAB, which can be ascribed to (i) formation of larger size of Cu(0) NPs in Cu/MIL-101 (see BFTEM image of Cu/MIL-101 given in **Fig. S4** in the Supporting Information) and (ii) the lower mass transfer limitations for Cu/nano-MIL-101 catalyzed liquid phase dehydrogenation of MeAB [67-69].

3.4. Effect of the copper concentration on the hydrogen generation rate of Cu/nano-MIL-101 catalyzed hydrolytic dehydrogenation of MeAB and the catalytic activity of Cu/nano-MIL-101 in the hydrolytic dehydrogenation of MeAB

The catalytic activity of Cu/nano-MIL-101 with various copper concentrations was investigated in the hydrolytic dehydrogenation of MeAB at room temperature to determine the effect of copper concentration on the dehydrogenation rate. **Fig. 7(a)** shows mole of evolved H₂/mole of MeAB versus time graph for Cu/nano-MIL-101 catalyzed dehydrogenation of MeAB at 25 °C for different copper concentrations. An almost linear hydrogen evolution starts immediately as the preformed catalyst was used. The *initial* rate of hydrogen generation was determined from the linear portion of the plot for each experiment. Expectedly, the hydrogen generation rate increases by the increase of copper concentrations ($k_{\text{obs}} = 0.0313, 0.0545$ and 0.1414 mol H₂/(mol MeAB×min.) for [Cu] = 0.86, 1.72 and 3.44 mM, respectively). The plot of hydrogen generation rate versus copper concentration, both on logarithmic scales, gives a straight line with a slope of 1.12 as shown in **Fig. 7(b)**. This result, within the experimental error, indicates that Cu/nano-MIL-101 catalyzed dehydrogenation of MeAB is first order with respect to the copper concentration.

It should also be noted that 3.44 mol % of catalyst can achieve the complete hydrolytic dehydrogenation of MeAB at room temperature under air. The initial activity of Cu/nano-MIL-101 was determined to be 257 mol H₂/mol Cu×h in the room temperature hydrolytic dehydrogenation of MeAB (see Supporting Information for the details of the initial TOF value determination). This activity value is higher than previously reported for the hydrolytic dehydrogenation of MeAB by not only non-precious metal based nanocatalyst Cu_{0.2}@Co_{0.8}/r-GO (138 mol H₂/mol metal×h) [26] but also precious metal used nanocatalyst systems such as Ag_{0.1}@Co_{0.45}Ni_{0.45}/r-GO (210 mol H₂/mol metal×h) [27].

3.5. Effect of the temperature on the hydrogen generation rate of Cu/nano-MIL-101 catalyzed hydrolytic dehydrogenation of MeAB and determination of activation parameters

Cu/nano-MIL-101 catalyzed dehydrogenation of MeAB was also carried out at different temperatures in the range 15-45 °C to investigate the effect of temperature on the hydrogen generation rate and to find activation parameters; activation energy (E_a), activation enthalpy (ΔH*) and entropy (ΔS*). The plot of mole of evolved H₂/mole of MeAB versus time graph for Cu/nano-MIL-101 catalyzed dehydrogenation of MeAB at various temperatures is given in **Fig. 8(a)**, as expected the rate of hydrogen generation is enhanced by the increase of the reaction temperature. The observed rate constants were found to be $k_{\text{obs}} = 0.0226, 0.0545, 0.1525$ and 0.4067 mol H₂/(mol MeAB×min.) at 15, 25, 35 and 45 °C, respectively.

These observed rate constants (k_{obs}) were used to construct the Arrhenius and Eyring-Polanyi plots given in Fig. 9(b) and (c), respectively. From the slope of the Arrhenius plot the activation energy (E_a) for the Cu/nano-MIL-101 catalyzed dehydrogenation of MeAB was found to be 34.1 kJ/mol. This value is lower than those of obtained by Cu_{0.2}@Co_{0.8}/r-GO (55.9 kJ/mol) [26], Ru@Ni/r-GO (37 kJ/mol) [29], Ru/MCM-41 (47.6 kJ/mol) [30] catalysts in the hydrolytic dehydrogenation of MeAB. The activation enthalpy (ΔH^*) and entropy (ΔS^*) values were determined from the Eyring-Polanyi plot given in Fig. 9(c), from this plot these values were determined as $\Delta H^* = 71.3$ kJ/mol and $\Delta S^* = -29.1$ J/(mol×K). The high positive value of ΔH^* and negative value of ΔS^* implies the presence of an associative mechanism in the transition state [70].

3.6. Effect of the nature of support material on the catalytic activity of guest Cu NPs in the hydrolytic dehydrogenation of MeAB

The uniqueness of Cu/nano-MIL-101 nanocatalyst among the different solid supported copper nanoparticles prepared by the same synthesis protocol was also tested by using the most commonly used solid support materials; silica (SiO₂), alumina (Al₂O₃) and carbon (C) in the hydrolytic dehydrogenation of MeAB under the identical conditions (under air at 25 °C) and their results were given in Fig. 9. The *initial* TOF values were found to be 85 (82 % conversion), 74 (68 % conversion), and 50 (45 % conversion) mol H₂/mol Cuxh for Cu/Al₂O₃, Cu/ SiO₂ and Cu/C catalysts, respectively. The low activity and conversion values obtained by these support materials can be explained by the clumping of surface bound Cu(0) NPs. BFTEM images of Cu/Al₂O₃, Cu/ SiO₂ and Cu/C catalysts (see Fig. S5-S7 in the Supporting Information) reveal that the existence of clumped Cu(0) NPs and some Cu(0) agglomerates on the surface of these solid support materials. The interaction between nano-MIL-101 framework and surface bound Cu(0) NPs might be strong enough to prevent the surface agglomeration of these particles. This kind of strong interaction between metal NPs and solid support materials has recently been named as “Strong Metal-Molecular Support Interaction” (SMMSI) by Yadav and co-workers [71]. Understanding the existing synergistic effects between the metal and nano-MIL-101 support remains an active area of research in our group.

3.7. Catalytic stability of Cu/nano-MIL-101 in the hydrolytic dehydrogenation of MeAB

The catalytic stability of Cu/nano-MIL-101 was examined by testing the recyclability performance of Cu/nano-MIL-101 in the hydrolytic dehydrogenation of MeAB. In the recyclability experiments, fresher aqueous MeAB was added into the reaction solution when all MeAB from the previous run was converted to H₂ and CH₃NH₂BO₂ and by this way, the reaction was continued up to ten consecutive cycles. As given in Fig. 10, Cu/nano-MIL-101 nanocatalyst provides complete conversion in MeAB dehydrogenation by retaining 83 % of its inherent catalytic activity even at 10th

recycle, which corresponds to the lower limit of total turnover number (TTON) of 872 (see Supporting Information for the details of the lower limit of TTON determination).

The morphological investigation of the recovered catalyst from 10th recycle was performed by BFTEM analysis. The inspection of BFTEM image (Fig. S8, Supporting Information) of recovered catalyst revealed that clumping of nano-MIL-101 support material and guest Cu(0) NPs. Additionally, P-XRD analysis of the same material indicative of slight distortion of the crystallinity of the host material nano-MIL-101 (Fig. S8, Supporting Information). The results of these two analyses explain the observed slight decrease in the catalytic activity at 10th recycle. The leaching possibility of Cu(0) NPs from nano-MIL-101 framework to reaction solution throughout the recyclability experiments, was also investigated by performing ICP-OES analyses on aliquots of the reaction solutions taken at the end of 1st, 5th and 10th recycle, in which no Cu was detected confirming that the retention of Cu(0) NPs on nano-MIL-101 framework. Taking all results together, one can conclude that Cu/nano-MIL-101 acts as highly durable nanocatalyst against leaching, sintering and clumping, which makes it a highly efficient and recyclable heterogeneous catalyst for the hydrolytic dehydrogenation of MeAB.

4. Conclusions

In summary, Cu(0) NPs stabilized by nano-MIL-101 framework (Cu/nano-MIL-101), have been successfully fabricated with high reproducibility and characterized through multi-pronged analyses, by using advanced analytical tools. This new Cu/nano-MIL-101 nanocatalyst shows remarkable catalytic activity (*initial* TOF = 257 mol H₂/mol Cuxh) in the hydrolytic dehydrogenation of MeAB under mild reaction conditions (under air at room temperature). Moreover, Cu/nano-MIL-101 nanocatalyst provides exceptional catalytic stability against to leaching, sintering and clumping throughout the recyclability experiments. This uniquely active, selective, and stable catalytic architecture presents itself as an excellent contender for clean hydrogen production, via room-temperature hydrolytic dehydrogenation of MeAB, and has a strong potential to be exploited in practical/technological applications, where MeAB is utilized as a viable hydrogen carrier in mobile fuel cell applications

Acknowledgments

Authors thanks to the Research Fund of Yüzüncü Yıl University Office of Scientific Research Project (FOA-2016-5376). Additionally, the partial supports by Fevzi Akkaya Scientific Activities Support Fund (FABED), Science Academy, and Turkish Academy of Sciences (TUBA) are gratefully acknowledged.

References

- [1] W. Mcdowall, M. Eames, Energy Policy 34 (2006) 1236–1250.

- [2] J. Hetland, G. Mulder, *Int J Hydrogen Energy* 32 (2007) 736-747.
- [3] J. A. Turner, *Science* 305 (2004) 972-974.
- [4] G. M. Whitesides, G. W. Crabtree, *Science* 315 (2007) 796-798.
- [5] Targets for Onboard Hydrogen Storage Systems for Light-Duty Vehicles, U.S. Department of Energy, <http://energy.gov/eere/fuelcells/downloads/doetargets-onboard-hydrogen-storage-systems-light-duty-vehicles>.
- [6] N. Muradov, T. Veziroglu, *Int. J. Hydrogen Energy* 30 (2005) 225-237.
- [7] L. Schlapbach, A. Züttel, *Nature* 414 (2001) 353-358.
- [8] J. Turner, G. Sverdrup, K. Mann, P. G. Maness, B. Kroposki, M. Ghirardi, R. J. Evans, D. Blake, *Int. J. Energy Res.* 32 (2008) 379-386.
- [9] S. H. Lim, J. Luo, Z. Zhong, W. Ji, J. Lin, *Inorg Chem.* 44 (2005) 4124-4126.
- [10] J. Weitkamp, M. Fritz, S. Ernst, *Int J. Hydr. Energ.* 20 (1995) 967-973.
- [11] N. B. McKeown, P. M. Budd, *Chem. Soc. Rev.* 35 (2006) 675-690.
- [12] N. L. Rossi, J. Eckert, M. Eddaoudi, D. T. Vodak, J. Kim, M. O'Keefe, O. M. Yaghi, *Science* 300 (2003) 1127-1134.
- [13] M. Au, A. Jurgensen, *J. Phys. Chem. B.* 110 (2006) 7062-7067.
- [14] M. Zahmakiran, S. Özkar, *Langmuir* 25 (2009) 2667-2676.
- [15] E. Rönnebro, E. H. Majzoub *J. Phys. Chem. B.* 111 (2007) 12045-12052.
- [16] H. L. Jiang, S. K. Singh, J. M. Yan, X. B. Zhang, Q. Xu, *Chem Sus. Chem.* 3 (2010) 541-548.
- [17] H. L. Jiang, Q. Xu, *Catal. Tod.* 170 (2011) 56-63.
- [18] T. Umegaki, J. M. Yan, X. B. Zhang, H. Shioyama, N. Kuriyama, Q. Xu, *Int. J. Hyd. Energ.* 34 (2009) 2303-2311.
- [19] M. Yadav, Q. Xu, *Energ. Environ. Sci.* 5 (2012) 9698-9725.
- [20] S. Karahan, M. Zahmakiran, S. Özkar, *Int. J. Hyd. Energ.* 36 (2011) 4958-4964.
- [21] Y. Yamamoto, K. Miyamoto, J. Umeda, Y. Nakatani, T. Yamamoto, N. Miyaura, *J. Organomet. Chem.* 691 (2006) 4909-4917.
- [22] M. E. Bowden, I. W.M. Brown, G. J. Gainsford, H. Wong, *Inorg. Chim. Acta* 2008 (361) 2147-2153.
- [23] A. Staubitz, M.E. Sloan, A.P.M. Robertson, A. Friedrich, S. Schneider, P.J. Gates, J. Schmedt, I. Manners, *J. Am. Chem. Soc.* 132 (2010) 13332-13345.
- [24] Z. X. Yang, F. Y. Cheng, Z. L. Tao, J. Liang, J. Chen, *Int. J. Hyd. Energ.* 37 (2012) 7638-7644.
- [25] L. Yang, W. Luo, G. Cheng, *ACS Appl. Mater. Int.* 5 (2013) 8231-8240.
- [26] Y. Du, N. Cao, L. Yang, W. Luo, G. Cheng, *New J. Chem.* 37 (2013) 3035-3042.
- [27] L. Yang, J. Su, X. Meng, W. Luo, G. Cheng, *J. Mater. Chem. A* 1 (2013) 10016-10023.
- [28] N. Cao, J. Sub, W. Luo, G. Cheng, *Catal. Commun.* 43 (2014) 47-51.
- [29] N. Cao, J. Su, W. Luo, G. Cheng, *Int. J. Hyd. Energ.* 39 (2014) 426-435.

- [30] L. Wen, Z. Zheng, W. Luo, P. Cai, G-Z Cheng, *Chin. Chem. Lett.* 26 (2015) 1345-1350.
- [31] F. Anke, D. Han, M. Klahn, A. Spannenberg, T. Beweries, *Dalton Trans.* 46 (2017) 6843-6847.
- [32] M. Zahmakiran, S. Ozkar, *Nanoscale* 3 (2011) 3462-3481.
- [33] B. L. Cushing, L. Kolesnichenko, C. J. Connor, *Chem. Rev.* 104 (2004) 3893-3996.
- [34] S. Ozkar, R. G. Finke, *J. Am. Chem. Soc.* 124 (2002) 5796-5895.
- [35] M. Zahmakiran, S. Ozkar, *Langmuir* 24 (2008) 7065-7067.
- [36] M. Zahmakiran, S. Ozkar, *Langmuir* 25 (2009) 2667-2678.
- [37] E. Castillejos, P. J. Debouttine, L. Roiban, A. Solhy, V. Martinez, Y. Kihn, O. Ersen, K. Philippot, B. Chaudret, P. Serp, *Angew. Chem. Int. Ed.* 48 (2009) 2529-2531.
- [38] M. Yurderi, A. Bulut, M. Zahmakiran, M. Kaya, *App. Catal. B Env.* 160 (2014) 514-524.
- [39] M. Zahmakiran, Y. Tonbul, S. Ozkar, *Chem. Commun.* 46 (2010) 4788-4790.
- [40] M. Zahmakiran, Y. Roman-Leshkov, Y. Zhang, *Langmuir* 28 (2012) 60-65.
- [41] R. J. White, R. Luque, V. L. Budain, J.H. Clark, D. J. Macquarrie, *Chem. Soc. Rev.* 38 (2009) 481-497.
- [42] J. Y. Lee, O. K. Farha, J. Roberts, K. A. Scheidt, S. T. Nguyen, J. T. Hupp, *Chem. Soc. Rev.* 38 (2009) 1450-1465.
- [43] A. Corma, H. Garcia, F. X. L. Xamena, *Chem. Rev.* 110 (2010) 4606-4625.
- [44] J. L. C. Rowsell, O. M. Yaghi, *Mic. Mes. Mater* 73 (2004) 3-10.
- [45] G. Ferey, C. M. Draznieks, C. Serre, F. Millange, J. Dutour, S. Surble, I. Margilowski, *Science* 309 (2005) 2040-2051.
- [46] M. Y. Masoomi, A. Morsali, P. C. Junk, *CrystEngComm* 17 (2015) 686-692.
- [47] S. Abedi, A. Morsali, *ACS Catal.* 4 (2014) 1398-1403.
- [48] R. Ricco, L. Malfatti, M. Takahashi, A. J. Hilla, P. Falcaro, *J. Mater. Chem. A* 1 (2013) 13033-13045.
- [49] M. Bellusci, P. Guglielmi, A. Masi, F. Padella, G. Singh, N. Yaacoub, D. Peddis, D. Secci, *Inorg. Chem.* 57 (2018) 1806-1814.
- [50] G. Li, H. Kobayashi, J. M. Taylor, R. Ikeda, Y. Kubota, K. Kenichi, M. Takata, T. Yamamoto, S. Toh, S. Matsumura, H. Kitagawa, *Nature Mater.* 13 (2014) 802-806.
- [51] E. Zanchetta, L. Malfatti, R. Ricco, M. J. Styles, F. Lisi, C. J. Coghlan, C. J. Doonan, A. J. Hill, G. Brusatin, P. Falcaro, *Chem. Mater.* 27 (2015) 690-699.
- [52] P. Falcaro, R. Ricco, A. Yazdi, I. Imaz, S. Furukawa, D. Maspoth, R. Ameloot, J. D. Evans, C. J. Doonan, *Coord. Chem. Rev.* 307 (2016) 237-254.
- [53] I. E. Ertas, M. Gulcan, M. Yurderi, A. Bulut, M. Zahmakiran, *J. Mol. Catal. A: Chem.* 410 (2015) 209-220.
- [54] I. E. Ertas, M. Gulcan, M. Yurderi, A. Bulut, M. Zahmakiran, *Mic. Mes. Mater.* 226 (2016) 94-103.
- [55] M. Zahmakiran, Y. Tonbul, S. Ozkar, *J. Am. Chem. Soc.* 132 (2010) 6541-6549.

- [56] A. Aijaz, A. Karkamkar, A. J. Choi, N. Tsumori, E. Rönnebro, T. Autrey, H. Shioyama, Q. Xu, *J. Am. Chem. Soc.* 134 (2012) 13926–13929.
- [57] Q. L. Zhu, J. Li, Q. Xu, *J. Am. Chem. Soc.* 135 (2013) 10210–10213.
- [58] L. Bromberg, Y. Diao, H. Wu, S. A. Speakman, T. A. Hatton, *Chem. Mater.* 24 (2012) 1664-1675.
- [59] D. Jiang, A. D. Burrows, K. J. Edler, *CrysEngComm* 13 (2011) 6916-6919.
- [60] M. Yurderi, A. Bulut, M. Zahmakiran, M. Gulcan, S. Ozkar, *App. Catal. B Env.* 160 (2014) 534-541.
- [61] B. K. Park, S. Jeong, D. Kim, J. Moon, S. Lim, J. S. Kim, *Journal of Colloid and Interface Science* 311 (2007) 417–424.
- [62] M. Yurderi, A. Bulut, I. E. Ertas, M. Zahmakiran, M. Kaya, *App. Catal. B Env.* 165 (2015) 169-175.
- [63] A. Bulut, M. Yurderi, I. E. Ertas, M. Celebi, M. Zahmakiran, M. Kaya, *App. Catal. B Env.* 164 (2015) 324-333.
- [64] S. Storck, H. Bretinger, W. F. Maier, *Appl. Catal. A* 174 (1998) 137-144.
- [65] R. S. H. Mikhail, S. Brunauer, E. E. Bodor, *J. Colloid Interface Sci.* 26 (1968) 45-52.
- [66] Z. Lu, L. Schweighauser, H. Hausmann, H. A. Wegner, *Angew. Chem. Int. Ed.* 2015 (54) 15556-15559.
- [67] D. E. Mears, *Ind. Eng. Chem. Process Des. Develop.* 10 (1971) 541-547.
- [68] J. K. Chinthaginjala, K. Seshan, L. Lefferts, *Ind. Eng. Chem. Res.* 46 (2007) 3968-3978.
- [69] A. Zamaniyana, Y. Mortazavi, A. A. Khodadadi, A. N. Pour, *J. Energ. Chem.* 22 (2013) 795-803.
- [70] K. A. Connors, *Theory of Chemical Kinetics*; VCH Publishers: New York (1990).
- [71] M. Yadav, T. Akita, N. Tsumori and Q. Xu, *J. Mater. Chem.* 22 (2012) 12582-12589.

Figure Captions

Fig. 1 P-XRD patterns of nano-MIL-101, Cu/nano-MIL-101 (1) (1.09 % wt Cu), Cu/nano-MIL-101 (2) (2.18 % wt Cu) and Cu/nano-MIL-101 (3) (4.12 % wt Cu) samples in the region of $2\theta = 2-40^\circ$.

Fig. 2 (a) Survey XPS spectrum of Cu/nano-MIL-101 in the region of $B_E = 1100-0$ eV, (b) Cu 2p core level high resolution-XPS (HR-XPS) spectrum of Cu/nano-MIL-101 in the region of $B_E = 940-925$ eV.

Fig. 3 Nitrogen adsorption–desorption isotherms of nano-MIL-101 and Cu/nano-MIL-101 (2.18 % wt Cu) samples.

Fig. 4 (a)-(d) BFTEM images of Cu/nano-MIL-101 (2.18 % wt Cu) sample in different magnifications and inset in (c) HAADF-STEM image of the selected region labelled as white colored square in (c).

Fig. 5 The plot of mole of evolved H_2 /mole of MeAB versus time graph for the hydrolytic dehydrogenation of MeAB ($[MeAB] = 100$ mM in 10.0 mL H_2O) catalyzed by Cu/nano-MIL-101 samples with different copper loadings in the range of 1.09–4.12 wt % (in all $[Cu] = 3.44$ mM) at room temperature.

Fig. 6 The plot of mole of evolved H_2 /mole of MeAB versus time graph for the hydrolytic dehydrogenation of MeAB ($[MeAB] = 100$ mM in 10.0 mL H_2O) catalyzed by Cu/nano-MIL-101 and Cu/MIL-101 samples (in all $[Cu] = 3.44$ mM) at room temperature.

Fig. 7 The plot of mole of evolved H_2 /mole of MeAB versus time graph for the hydrolytic dehydrogenation of MeAB ($[MeAB] = 100$ mM in 10.0 mL H_2O) catalyzed by Cu/nano-MIL-101 with different copper concentrations at room temperature.

Fig. 8 (a) The plot of mole of evolved H_2 /mole of MeAB versus time graph for the hydrolytic dehydrogenation of MeAB ($[MeAB] = 100$ mM in 10.0 mL H_2O) catalyzed by Cu/nano-MIL-101 (in all $[Cu] = 1.72$ mM) at different temperatures, (b) Arrhenius plot and (c) Eyring-Polanyi plot.

Fig. 9 The plot of mole of evolved H₂/mole of MeAB versus time graph for the hydrolytic dehydrogenation of MeAB ([MeAB] = 100 mM in 10.0 mL H₂O) catalyzed by Cu/nano-MIL-101 (2.18 % wt Cu), Cu/Al₂O₃ (2.17 % wt Cu), Cu/ SiO₂ (2.32 % wt Cu) and Cu/C (2.12 % wt Cu) catalysts (in all [Cu] = 3.44 mM) at room temperature.

Fig. 10 The plot of mole of evolved H₂/mole of MeAB versus time graph for 1st, 5th and 10th recycle in the Cu/nano-MIL-101 ([Cu] = 3.44 mM) catalyzed hydrolytic dehydrogenation of MeAB ([MeAB] = 100 mM in 10.0 mL H₂O) at room temperature.

Fig. 1

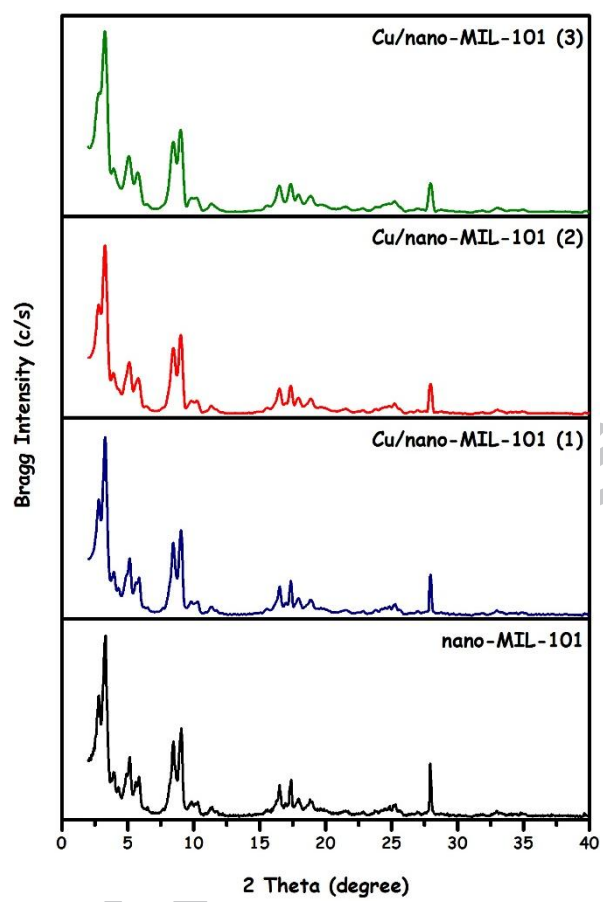


Fig. 2

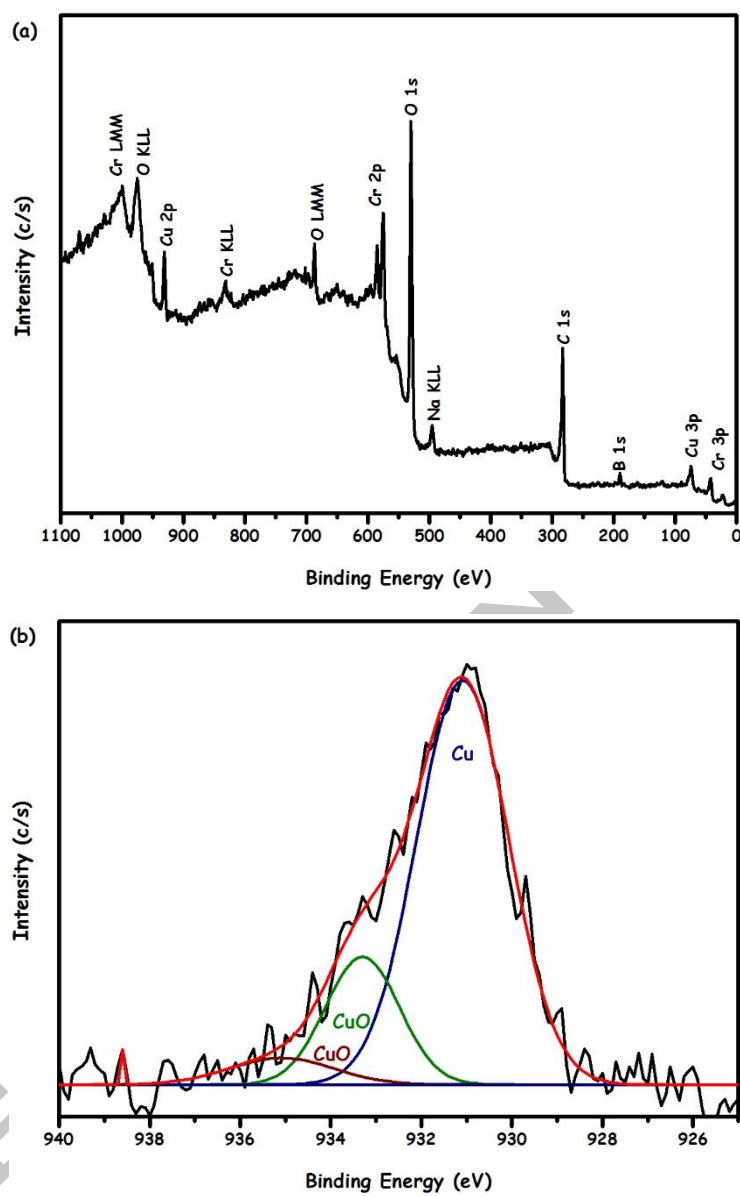


Fig. 3

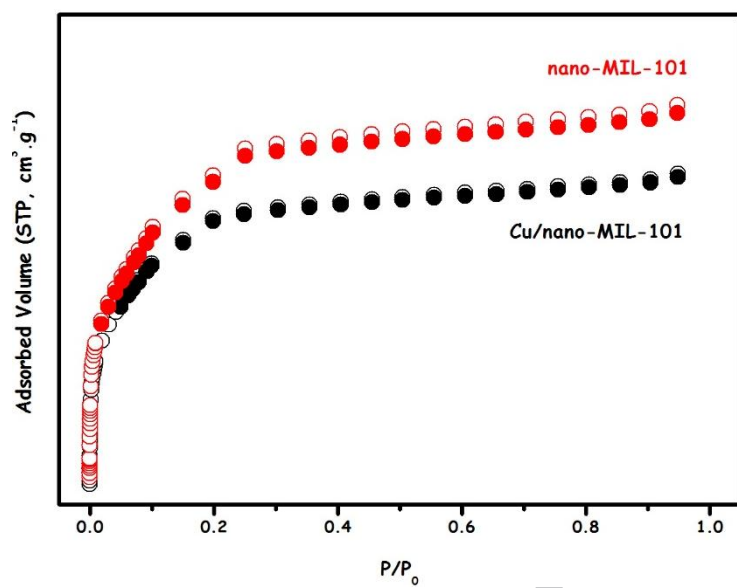


Fig. 4

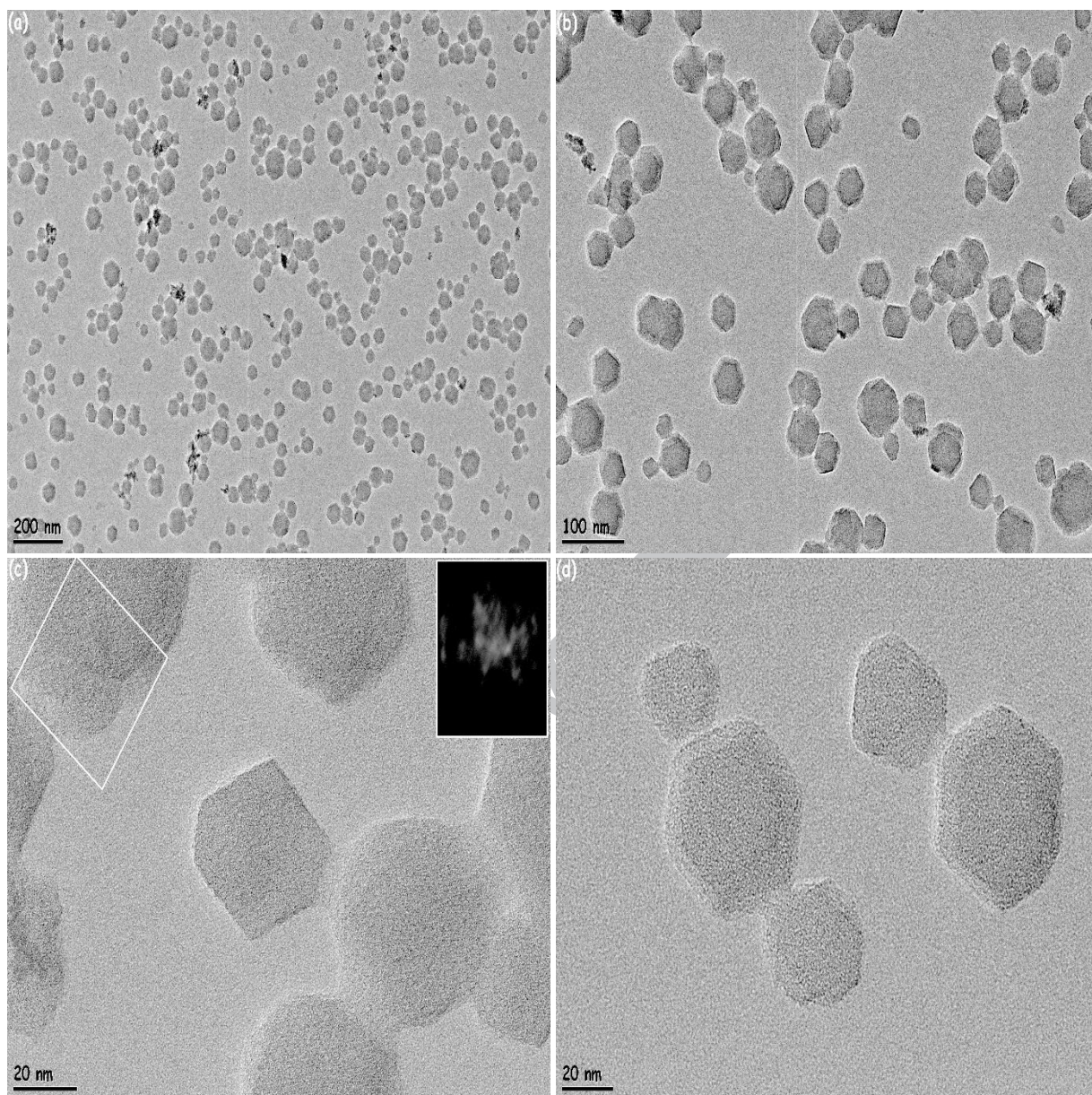


Fig. 5

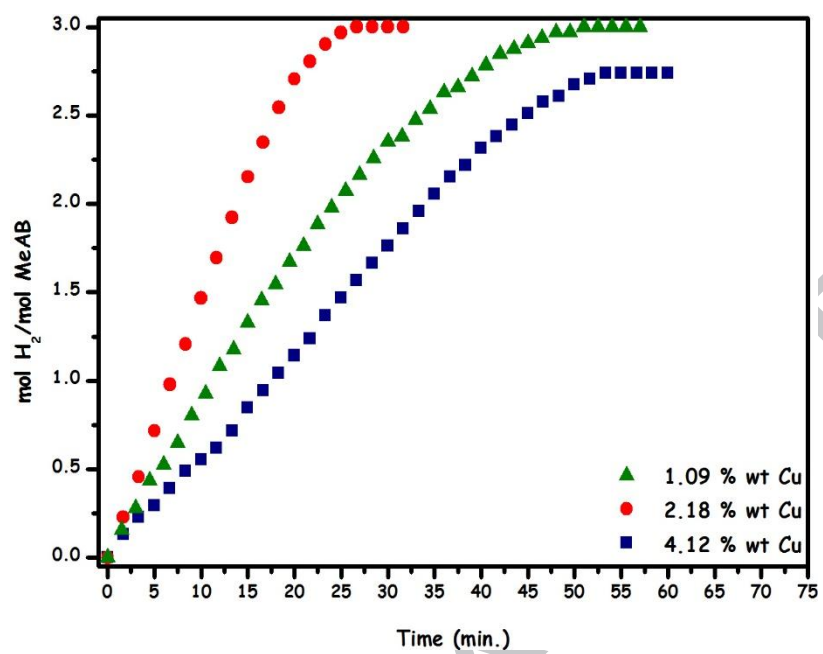


Fig. 6

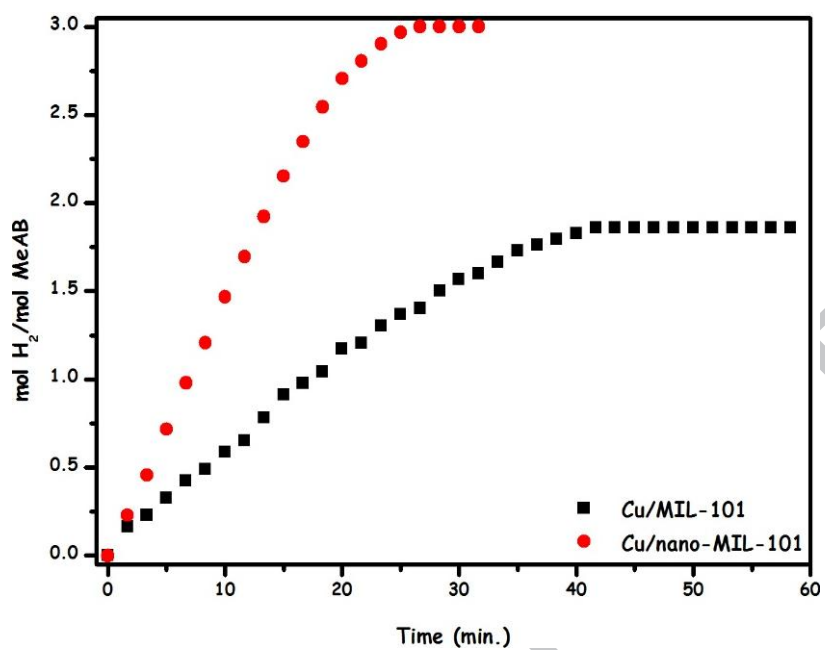


Fig. 7

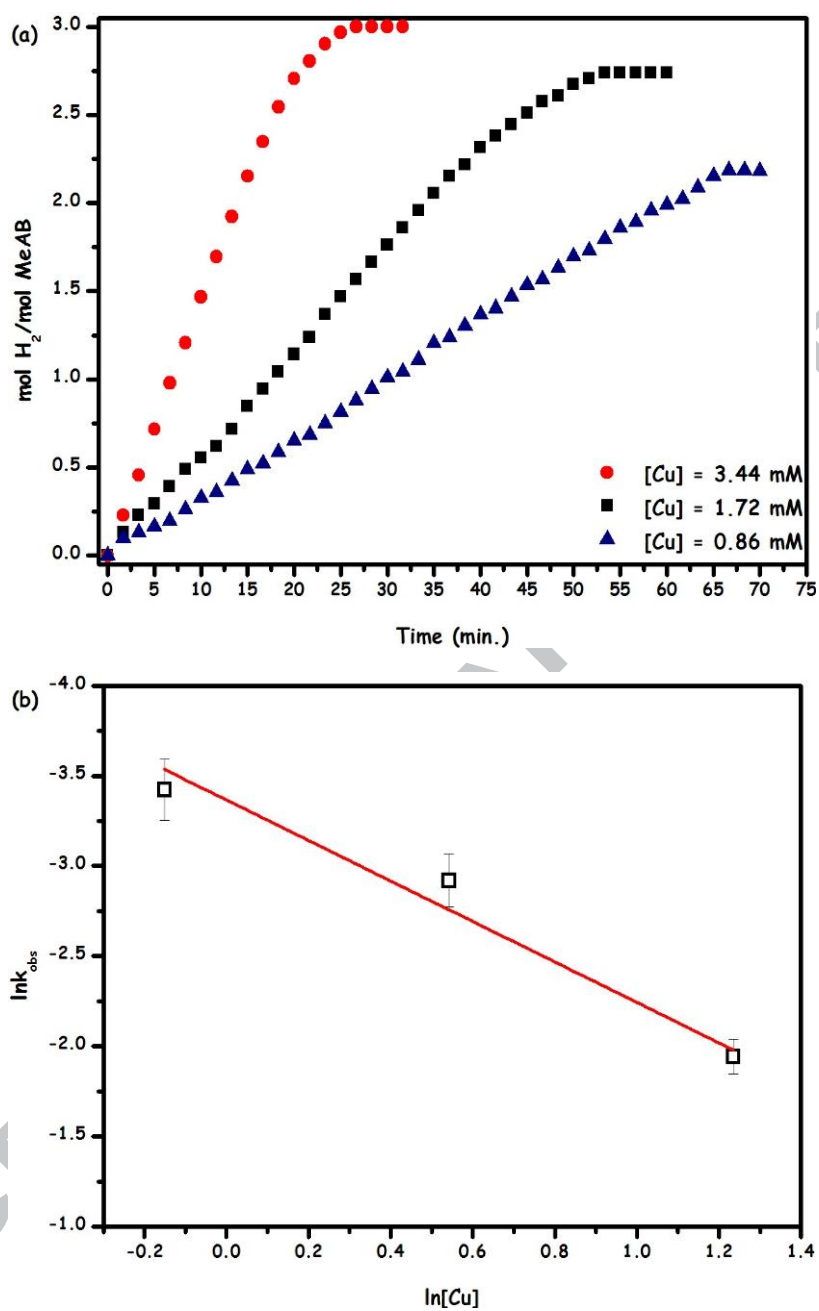
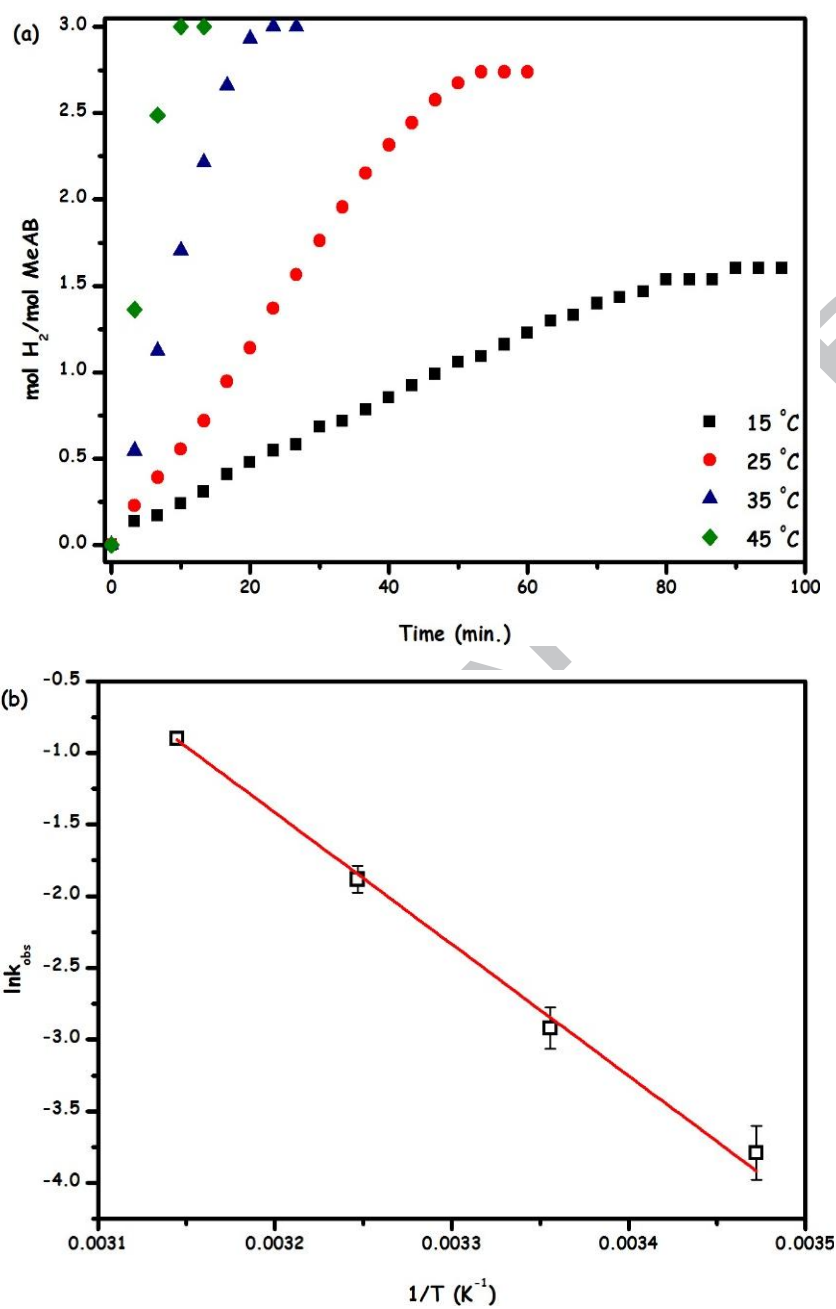


Fig. 8



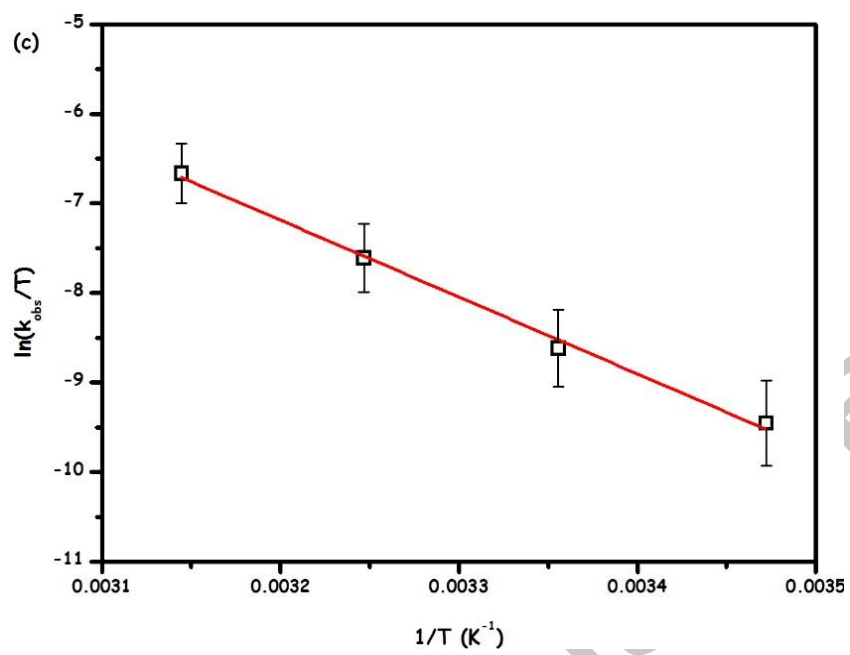


Fig. 9

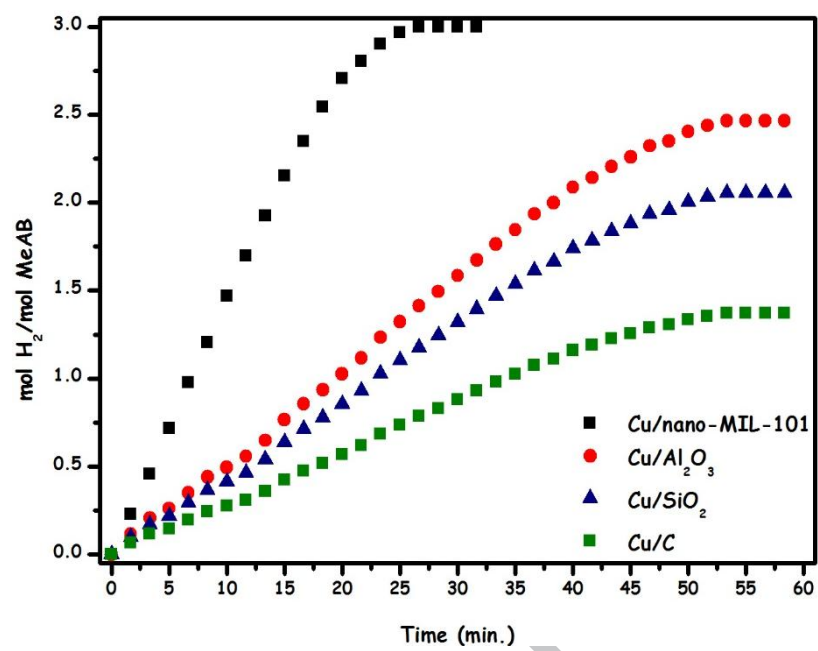
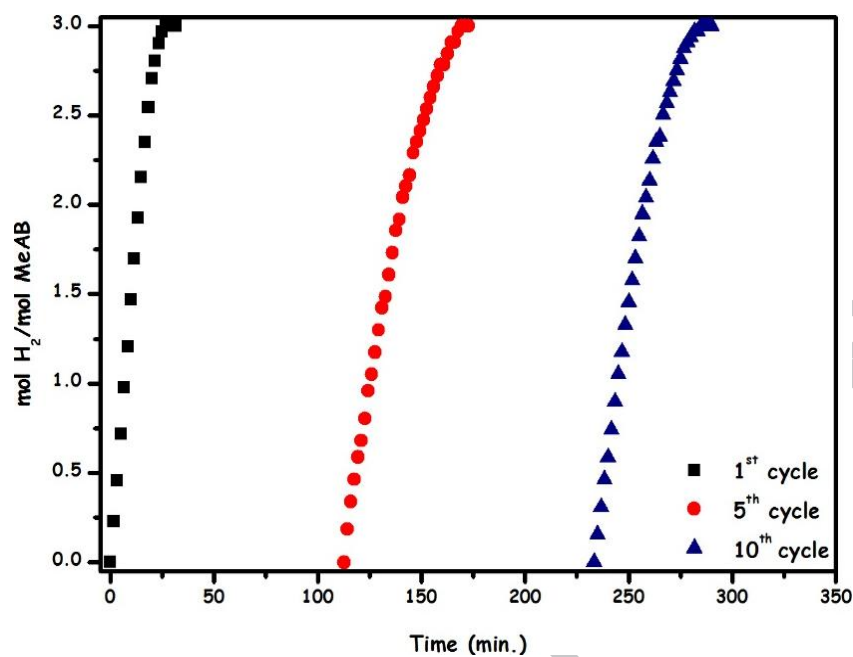
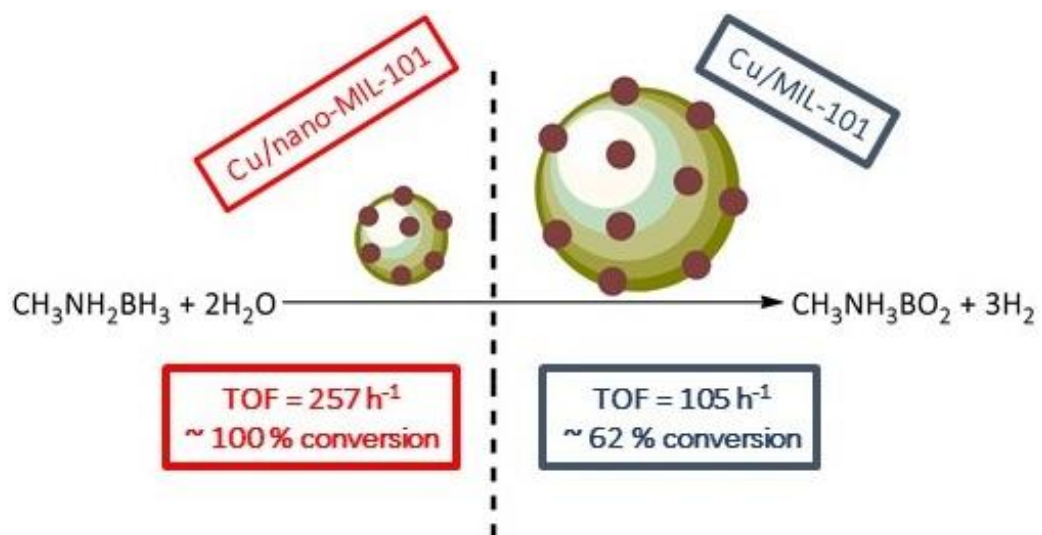


Fig. 10

**Highlights:**

- Cu/nano-MIL-101 nanocatalyst has reproducibly been synthesized and characterized by using advanced analytical techniques,
- Cu/nano-MIL-101 nanocatalyst was used in the hydrolytic dehydrogenation of MeAB at room temperature,
- This new catalyst provides remarkable catalytic activity **TOF = 257 mol H₂/mol Cu×h) and conversion (> 99 %) under air at room temperature.**



ACCEPTED MANUSCRIPT